



HAL
open science

Starch-fibers composites, a study of all-polysaccharide foams from microwave foaming to biodegradation

Ana Isabel Quilez-Molina, Jean François Le Meins, Bertrand Charrier, Michel Dumon

► **To cite this version:**

Ana Isabel Quilez-Molina, Jean François Le Meins, Bertrand Charrier, Michel Dumon. Starch-fibers composites, a study of all-polysaccharide foams from microwave foaming to biodegradation. Carbohydrate Polymers, 2024, 328, pp.121743. 10.1016/j.carbpol.2023.121743 . hal-04398152

HAL Id: hal-04398152

<https://hal.science/hal-04398152v1>

Submitted on 16 Jan 2024

HAL is a multi-disciplinary open access archive for the deposit and dissemination of scientific research documents, whether they are published or not. The documents may come from teaching and research institutions in France or abroad, or from public or private research centers.

L'archive ouverte pluridisciplinaire **HAL**, est destinée au dépôt et à la diffusion de documents scientifiques de niveau recherche, publiés ou non, émanant des établissements d'enseignement et de recherche français ou étrangers, des laboratoires publics ou privés.



Distributed under a Creative Commons Attribution - NonCommercial - NoDerivatives 4.0 International License

1
2 **Starch-fibers composites, a study of all-polysaccharide foams from**
3 **microwave foaming to biodegradation**

4
5 *Ana Isabel Quilez-Molina^{1,2,*}, Jean François Le Meins¹, Bertrand Charrier³, Michel Dumon^{1,*}*
6

7 ¹Laboratoire de Chimie des Polymères Organiques, Univ. Bordeaux, CNRS, Bordeaux INP, LCPO UMR 5629,
8 F-33607 Pessac (France).

9 ²BioEcoUVA Research Institute on Bioeconomy, University of Valladolid (Spain)

10 ³University of Pau and the Adour Region, E2S UPPA, CNRS, Institute of Analytical Sciences and Physico-
11 Chemistry for the Environment and Materials-Xylomat, (IPREM-UMR5254), 40004, Mont de Marsan, France.
12

13 **E-mail address of each author:**

14 Ana Isabel Quilez-Molina*: anaquilezm@gmail.com; (+34606069490)

15 Jean François Le Meins: lemeins@enscbp.fr

16 Bertrand Charrier: bertrand.charrier@univ-pau.fr

17 Michel Dumon: michel.dumon@u-bordeaux.fr; (+33625070385)
18

19 **Abstract**

20 Sustainable composite foams based on rice starch and cellulosic long microfibers were successfully fabricated
21 using microwave irradiation. They were presented as a promising method to recycle some of the textile industry
22 waste. A deep study of the processability and functionality of the composites revealed the performance
23 improvement of starch with the addition of long cellulosic microfibers, especially with 6 wt.% of Arbocel[®], in
24 terms of foamability, water, and mechanical resistance features. Moreover, sodium bicarbonate, which acted as
25 a blowing and pulping agent, led to a lower density and better fiber distribution that resulted in an improvement
26 of the foams' functionalities. The range of the study is new in the domain of long microfiber foam composites
27 in terms of foaming capability, and mechanical, thermal, and water resistance properties. Furthermore, all foams
28 showed excellent biodegradability properties against a fungus commonly found in the environment; for example,
29 values around 60% weight loss after 33 days. Finally, the assessment of the CO₂ emission during the process
30 underlines the environmental benefits of the method employed.
31

32 **Keywords:** Flax, cellulose, pulping, microwave, long microfibers, starch composites, bio-based foams
33

34 **1. Introduction**

35 In “dynamic” foamable systems, the cumulation of several properties (lower weight, water sensitivity,
36 mechanical strength, biodegradability) is indeed a difficulty. Many factors and mechanisms compete and interact
37 in opposite or synergetic ways: initial viscosity; fiber type, content, and length; as well as interactions between
38 components of the formulation, in particular, via a competitive behavior of H-bonding between the numerous
39 hydroxyl bonds (cellulose, water, starch).

40 On the other hand, all polysaccharide foam composites filled with long continuous or discontinuous cellulose
41 microfibers represent a sustainable way to carry out the recycling of textile fibers. Indeed, the textile industry is
42 considered the fifth largest contributor to carbon emissions, producing 10 % of the total carbon emissions
43 (Juanga-Labayen et al., 2022). Regarding waste management, 75-85 % of the textile waste is disposed of in
44 landfills, 25-15 % is reused or recycled, and less than 1% is recycled back into clothing (Espinoza Pérez et al.,
45 2022; Mu & Yang, 2022; Négrier et al., 2023; Völtz et al., 2023). The residues of textile fibers can be
46 advantageously used as composite reinforcements providing better mechanical properties to the composite
47 (Bergel et al., 2021; van Rijswijk & Bersee, 2007). However, the reprocessing of fibers as fillers is often limited
48 by either the lack of impregnation with the matrix, low dispersibility, or lower thermal resistance for being
49 processable with many polymers (Bergel et al., 2021; van Rijswijk & Bersee, 2007). A great challenge of
50 reprocessing fiber tissues has been associated with the heterogeneous chemical composition present in textile
51 fibers, which arrangement, content, and concentration in different carbohydrates (i.e., cellulose, lignin,
52 hemicellulose, pectin) change with the type of tissue (Alam & Christopher, 2017; Foulk et al., 2006). For
53 example, cotton-like fibers are mainly composed of cellulose fibers (about 95 wt.%), while flax fibers are a self-
54 contained composite that consists of a bundle of cellulose fibers reinforced with non-cellulosic components, i.e
55 pectin (Foulk et al., 2006; Zimniewska et al., 2018). This result in different recycling pre-treatments that includes
56 some highly toxic and hazardous chemicals, such as carbon disulfide (CS₂) or ammonium (Alam & Christopher,
57 2017). Alkaline treatment is the most popular and cost-effective method to obtain high-performance natural
58 fibers and it is included in the recycling procedure of textile and paper fibers (Adu et al., 2018; H. Chen et al.,
59 2017). The basic pulping removes the hemicellulose and lignin, incrementing the availability of hydroxyl groups
60 present in cellulose to interact with a hydrophilic polymeric matrix (H. Chen et al., 2017).

61 The employment of sodium bicarbonate (NaHCO₃) as a basic pulping agent of cellulosic fibers, before loading
62 into a polymer matrix, is a sustainable strategy to pretreat the cellulosic fibers. In addition to this, NaHCO₃ has
63 been also widely employed to obtain low-density porous polymeric composites, acting as a blowing agent by
64 thermally degrading into CO₂, H₂O, and Na₂CO₃ (Bergel et al., 2021; Saed Hussein et al., 2019; Wei et al., 2023).

65 The foaming properties of NaHCO₃ were observed by (Saed Hussein et al., 2019), where this chemical reduced
66 the density of an epoxy resin obtained up to 3 times. This blowing agent has been employed to improve the
67 properties of sustainable polymeric materials, such as the bactericide properties of Materbi®-carvacrol
68 composites (Lopresti et al., 2019), or the expansion capability of starch-based foams (Georges et al., 2018; Robin
69 et al., 2010).

70 The great compatibility of starch with cellulosic compounds, derived from their chemistry, based on units of
71 glucose that form chains of amylopectin and amylose biopolymers, has been already proved in numerous articles
72 that include starch-based foams loaded with cellulosic-based fibers (Bergel et al., 2021; Ji et al., 2021; S. Peng
73 et al., 2022). These studies confirmed that fibers influence the foaming mechanism of starch, changing the size
74 and distribution of pores, and hence, their final properties. The foaming mechanism of starch starts with the
75 diffusion of water molecules into the amorphous region of the semicrystalline starch granules when the MW
76 heating conditions reach the gelatinization temperature (around 70 °C). This results in starch gelatinization (i.e.,
77 disruption of the molecular order of the starch granules), which includes the cleavage of intermolecular bonds,
78 structural rearrangements, and the formation of new interactions with the solvent. Afterwards, when the
79 temperature exceeds the boiling point of water, the inner moisture is transformed into superheated steam bubbles
80 that expand, creating a cellular structure and a solid foam (Soykeabkaew et al., 2015; Wani et al., 2012). Recently
81 published articles have already employed the characteristic properties of rice starch to create materials with
82 advanced properties, such as super absorbent foams (Q. Zhang et al., 2020), batteries (Escamilla-Pérez et al.,
83 2023), and which highlighted good performance properties in combination with cellulosic fibers (Almeida et al.,
84 2019; F. L. Chen et al., 2022). Moreover, rice starch is considered an important source of starch (about 80%),
85 cheaper and more available than other starch (Wani et al., 2012; Q. Zhang et al., 2020). Moreover, rice production
86 generates about 15-20 % of broken rice, commonly used for animal feeding, that can be used for developing new
87 materials, preventing the employment of other edible and more demanded starches (e.g., corn, cassava) for a
88 non-nutritional purpose (Wani et al., 2012; Q. Zhang et al., 2020)(F. Chen et al., 2019; Soykeabkaew et al., 2015;
89 Wani et al., 2012).

90 However, despite of high potential of starch foams to substitute petroleum-derived polymers in fields such as
91 food packaging and drug delivery systems (Soykeabkaew et al., 2015). Few studies include a complete analysis
92 of the effect of long cellulosic microfibers (>1 mm) on different parameters that can provide useful information
93 for the processability and applicability of the starch foams (S. Peng et al., 2022). According to them, the
94 improvement in the porosity, processability, and functional properties of starch foam composites (i.e.,
95 biodegradability and mechanical resistance) with the addition of long microfibers (neat or pulped with NaHCO₃)
96 is expected. Moreover, starch foaming is assisted by microwave irradiation, whose highly effective internal
97 heating reduces the exposure time and energy becoming an eco-friendly a save-costing manufacturing technique.
98 Moreover, the low exposure time, reduced from hours to minutes/seconds, is ideal for thermal-sensitive fillers
99 (Naik et al., 2022; Yu et al., 2021). Lastly, microwave irradiation can have a positive effect on enhancing the
100 pulping effect of alkaline reagents on fibers, as previously shown (Dong et al., 2022).

101 Sodium hydrogen carbonate (NaHCO₃) will be tested, as an edible and green chemical, to act as a pulping agent,
102 improving the dispersion and compatibility of the fibers with the starch matrix and as a blowing agent, promoting
103 the formation of pores and reducing the material density, obtaining cellulosic fibers-starch foams composites
104 with excellent functional properties. The effect of NaHCO₃ will reveal more noticeable in flax fibers as a result
105 of the removal of non-cellulosic components, despite that, all fibers (neat or pulped) enhanced the fibers'

106 dispersity, the expansion ratio, and reduced the water sensitivity of starch foams. Last but not least, the study of
 107 the environmental impact of these materials was performed by quantifying the composites' biodegradability and
 108 greenhouse gas emissions.

109 The overall objective is to provide a complete analysis, from processing to degradation, of all polysaccharide
 110 foam composites filled with long continuous or discontinuous cellulose **microfibers**; as new sustainable foam
 111 products using an eco-friendly and low-cost method.

112
 113 **2. Materials and methods**

114 *2.1 Materials*

115 Long discontinuous cellulose microfibers were kindly provided by JRS Rettenmaier (France): pure cellulose
 116 (99.5 % cellulose) Arbocel® FIF 400, labelled as A-F400, with an average length of 2000 μm and fiber diameter
 117 of 35 μm . Terre de Lin / Safilin (France) kindly provided flax yarns (labelled as F) from a textile wire spool,
 118 whose chemical composition was about 0.6-1.0 % pectin, 2.5-3.0 wt.% lignin, 70-80 wt.% cellulose and 14-20
 119 wt.% hemicellulose (Zimmiewska et al., 2018). The yarns of F fibers were carefully separated and cut in the same
 120 length as the container that will determine the final size of the foams (i.e., 3.4 cm), to fill the whole final foamed
 121 material with one “single” fibers’ network. Generally, a single flax fiber length varies from 4 mm to 80 mm, and
 122 a unitary fiber diameter of 20 micrometres which individual fibers are linked by pectin (Poilâne et al., 2014).
 123 Before mixing with starch and foaming, a bulk dry interweaved network of microfibers is realized. **Table 1**
 124 summarizes the main characteristics of the reinforcements (A-400 and F) used in this article. A native Rice starch
 125 (labelled as RS) was provided by Sigma Aldrich. Rice starch has been chosen because it possesses a high
 126 amylopectin/amylose ratio (17-29 % of amylose) that provides suitable expansion properties and low density to
 127 the foams. This occurs because amylopectin has better water-holding capacity, providing good swelling
 128 properties and sufficient strength to trap bubbles and create pores (F. Chen et al., 2019; Soykeabkaew et al.,
 129 2015; Wani et al., 2012). Moreover, its small granule size (about 3-8 μm) is known to provide a better mechanical
 130 performance in comparison with other starches with larger granules (Lee et al., 2009). The plasticizer glycerol
 131 was selected as a non-volatile plasticizer, increasing the durability of the polymer’s mechanical characteristics
 132 (Prabhakar et al., 2017).

133

| Cellulose fiber Reinforcement | Average Length (L) | Average Diameter (D) | Estimated average aspect ratio (L/D) | Content of cellulose (%) | Apparent bulk density (g/cm ³) |
|-------------------------------|-------------------------|---|--------------------------------------|--------------------------|--|
| A-F400 | 2000 μm | 35 μm | 57 | 99.5 | 0.025-0.05 |
| F | 3.4 cm = mold dimension | 20 μm is the average unitary filament diameter | ~1 700 | 70-80 | 1.5 |

134 **Table 1.** The labelling and characteristics of the long cellulosic microfibers. The data is provided by the suppliers.

135

2.2 Starch-cellulose composites foamed through microwave (MW) irradiation

The composite foams were obtained employing two different free-expansion fabrication methods adapted from Tacha S. *et al.*, (Tacha et al., 2023):

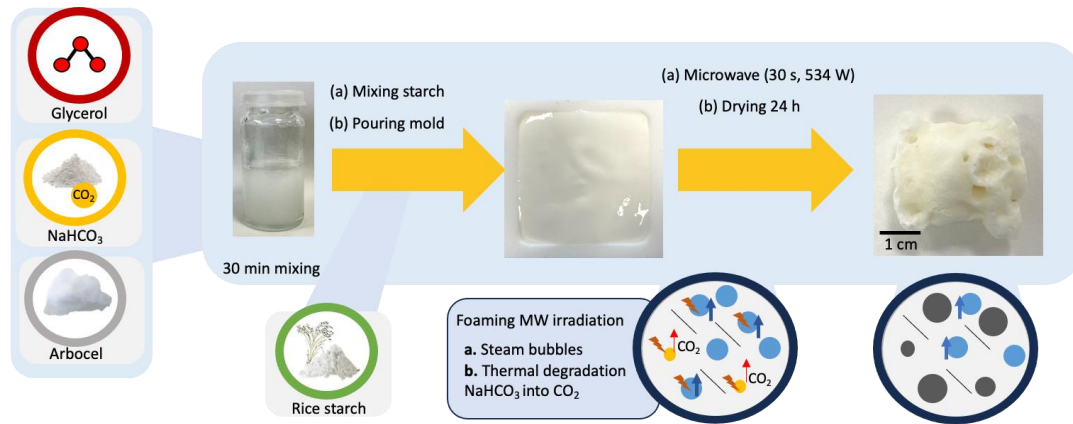
(a) Water as the only blowing agent

For the preparation of the materials, 2.8 g of the plasticizer glycerol was put to stir at 300 rpm in a hot plate (Hei-PLATE Mix 20) with 9.6 g of water (giving a solution at 22.6 wt.% of glycerol), for 5 min until obtaining a clear solution. Then, A-F400 was added in two different concentrations, 2 and 6 wt.% with respect to the starch, which was added in the last step. F fibers were prepared only in 2 wt.% because the 6 wt.% overcame the mould volume capacity, see **Fig. S1** of Supporting information. All these ingredients were mixed for 30 min at 700 rpm in the hot plate (Hei-PLATE Mix 20). Then, they were mixed in a manual mode with 11.4 g of RS to obtain a homogeneous and viscous starch batter, in which the concentration of starch in the mixing solution is 47.9 wt.%. This starch batter was subsequently poured into a mould of polytetrafluoroethylene (PTFE) (3.4 x 3.4 x 1.4 cm³) until the complete filling (~12 g). The PTFE mold was placed in a standard microwave (AYA MO-22 AL) for 30 s, at 534 W. The MW conditions (i.e., powers and time) were optimized to obtain the best foam expansion, avoiding the excessive heating that could result in the burn of the sample, see the photograph of the sample treated at 700 W for 45 s in **Fig. S2** of Supporting information). Finally, the product was carefully removed from the mould and the starch composite foam obtained was left to dry under the hood at room temperature for 24 hours to allow the evaporation of most of the remaining water molecules, ~30 wt.% for all samples, independently to the fiber type and concentration. The same values of water loss were observed in other starch foams enriched with cellulosic fibers (Lopez-Gil et al., 2015). Starch foams were kept in polyethylene (PE) zip bags until their characterization.

(b) Water and sodium bicarbonate as blowing agents

The scheme of **Figure 1** displays the production process of starch-composite foams using A-F400 filler as an example. Following the fabrication steps explained above, 2.8 g of glycerol and 0.57 g of hydrogen sodium carbonate or sodium bicarbonate NaHCO₃ (in water, the hydrogen carbonate ion HCO₃⁻), plasticizer, and foaming agent respectively, were put to stir at 300 rpm in 9.6 g of water for 5 min until obtaining a clear solution. Note that the global concentration in weight is not the same (21.6 wt.%) because of the presence of NaHCO₃. The basic character of the foaming agent sodium bicarbonate raised the pH to 8.5. Then, different quantities of the commercial cellulose fibers (2 and 6 wt.% regarding the starch fraction) were mixed with the previous solution for 30 min at 700 rpm (Hei-PLATE Mix 20). After manually mixing with 11.4 g of RS, the homogeneous batter was placed in a mould of polytetrafluoroethylene (PTFE) (3.4 x 3.4 x 1.4 cm³), and placed in a microwave (30 s, 534 W). As shown in the scheme of **Figure 1**, the starch-cellulose mixture filled the mould cavity, however, as a consequence of the expansion effect of the microwave irradiation, part of the foam flashed out of the mould. However, this effect was not undesirable because it facilitated the interpretation of the expansion capability of each sample. In the presence of NaHCO₃, the foaming involved two mechanisms: the formation and growth of

172 steam bubbles, observed also in the fabrication method explained above, and the thermal decomposition of
 173 NaHCO_3 , which thermal degradation results in the release of CO_2 gas (Tacha et al., 2023). Samples are labelled
 174 RS_xfiber-name_CO₃ which stands for RS: rice starch, x: mass percentage of fibers, F400: cellulose Arbocel[®]
 175 A-F400, F: flax, CO₃: addition of NaHCO_3 .
 176
 177



178
 179 **Figure 1.** The scheme of the fabrication process of starch-cellulose foams. The blue circles represented the steam
 180 bubbles, the yellow circle represented the sodium bicarbonate, the lines indicated the fibers and the orange
 181 lightning represented the microwave irradiation.

182

183 2.3 Foam starch composites characterization

184 2.3.1 Amylose content

185 The amylose content of rice starch used was measured at INRAE Nantes (Biopolymères Interactions
 186 Assemblages), Matériaux, Création & Comportement (MC2) by a calorimetric method, i.e. the enthalpy
 187 measurement of an amylose/lipid (LPC) complex. Amylose has a water content of 11% determined by
 188 thermobalance before DSC analysis. An 8% L- α -lysophosphatidylcholine (LPC) solution was prepared. Its
 189 enthalpy was calculated using the DSC Q200 apparatus (TA-waters instruments) using the method reported by
 190 (Mestres et al., 1996) with slight modifications: A 60 μL pan of starch water/LPC solution, against a 60 μL
 191 reference pan of pure water, was scanned by DSC. The temperature was increased up to 140°C at a rate of 10
 192 °C/min, followed by an isotherm of 2 min, and temperature was decreased to 20°C at a rate of 3 °C/min. This
 193 cycle was repeated two times. Upon heating, all amylose melts; upon cooling, all amylose crystallizes in the
 194 form of an amylose/LPC complex, which is then measured. Enthalpy obtained was calculated using the software
 195 TA Instrument Universal Analysis, obtaining $\Delta H = 6.809 \text{ J/g}$ at 89.26 °C, which corresponded to 25.5 % of
 196 amylose (average of two samples). The DSC curves are reported in **Figure S3** of Supporting information.

197

198 2.3.2 Apparent density and expansion ratio

199 The apparent density of the foams was calculated by dividing the masses by the volumes of the foams, in
200 triplicate for each sample. The density was calculated after 24 hours to allow the foam structure to dry and set
201 when most of the water molecules (in around 30 % of the total foam weight) were evaporated and following

202 **Equation 1:**

$$203 \text{ Foam density } \left(\frac{\text{g}}{\text{cm}^3} \right) = \frac{W_f}{V_f} (1)$$

204

205 Where w_f is the foam mass (g) and v_f is the foam volume (cm^3).

206

207 The expansion ratio was calculated following the equation **Equation 2**, as reported elsewhere (Gimeno et al.,
208 2004):

209

$$210 \text{ Expansion ratio} = \frac{V_f}{V_1} (2)$$

211

212 Where V_f is the volume of the pre-foamed batter and V_f is the volume of the foam after 24 hours of drying.

213

214 2.3.3 *Viscosity of initial formulation before foaming*

215 The rheological behaviour of the starch batter was measured using a stress-controlled rotational rheometer
216 (Anton Parr MCR302) plate geometry ($\varnothing=25\text{mm}$) was chosen with a gap around 1mm, regarding the
217 characteristic size of the cellulose fiber used at 20°C. In a first attempt shear rate sweeps were performed from
218 $0,01\text{s}^{-1}$ to 100s^{-1} to characterize the viscosity versus shear rate in a relatively large range of shear flow. This
219 protocol revealed complex behaviour that was not easily repeatable, probably because of stationary state issues
220 or thixotropy. Therefore, a constant shear rate during 2 min at different values (0.1; 0.5; 1.0, and 5.0 s^{-1}) was
221 applied in order to check whether the viscosity was measured in a steady state or not. Each measurement was
222 performed in triplicate.

223

224 2.3.4 *Scanning electron microscopy (SEM)*

225 The morphological study of the samples was performed using a scanning electron microscope (SEM) was
226 employed (model HITACHI S-3000N). For the preparation of the samples, foams frozen in liquid nitrogen and
227 fractured to ensure that the microstructure remained intact. Surfaces were coated with gold using a sputter coater
228 (model EMScope SC 500), in an argon atmosphere. The average cell size and cell density (number of cells per
229 volume unit) of the analyzed foams were calculated using the ImageJ software. Cell density was calculated using
230 the **Equation 3** following the method published elsewhere (Pinto et al., 2014):

231

232
$$N_f = \left(\frac{nM^2}{A}\right)^{3/2} \cdot \frac{1}{1 - V_f} \quad (3)$$

233 Being V_f calculated using the **Equation 4**:

234
$$V_f = 1 - \frac{\rho_f}{\rho_p} \quad (4)$$

235
236 Where N_f is the cell density (cells/cm³), n is the number of cells in the micrograph, M is the magnification of
237 the image, A is the area of the micrograph (cm²). V_f is the void fraction/porosity, ρ_f is the density of the foam
238 (g/cm³), and ρ_p is the density of the non-foamed starch (g/cm³), which corresponds to 1.50 g/cm³ (Yildirim et
239 al., 2014).

240

241 2.3.5 *Attenuated total reflection Fourier transform infrared (ATR-FTIR) spectroscopy*

242 Infrared spectra of the fibers and pulped fibers were obtained using an Attenuated Total Reflectance (ATR)
243 accessory (GladiATR, PIKE Technologies) coupled to a Fourier Transform Infrared (FTIR) spectrometer (Vertex
244 70, Bruker).

245

246 2.3.6 *Thermal properties*

247 The thermal gravimetric (TG) curves and the first derivative of the TGA curve (DTG) curve were acquired using
248 a TA Q500 instrument. The samples (~20 mg) were heated from 30 to 850 °C under an inert N₂ atmosphere with
249 a flow rate of 60 mL/min and a heating rate of 10 °C/min.

250

251 2.3.7 *Moisture content, Absorption isotherms at controlled RH (%), Liquid water absorption capability 252 and water-soluble fraction*

253 The moisture content was measured by introducing the samples with a weight (W_1) in a vacuum oven at 40 °C
254 until reaching constant weight (W_2) as reported in our previous work (Quilez-Molina et al., 2023). The moisture
255 content was calculated following the **Equation 5**:

256
$$\text{Moisture (\%)} = \frac{W_1 - W_2}{W_1} \times 100 \quad (5)$$

257

258 Absorption isotherms were determined through a static gravimetric method by setting different relative humidity
259 (RH) conditions: 43%, 59%, and 100%. The controlled relative humidity was obtained by placing the samples
260 (1.5 cm x 1.5 cm) in sealed jars with small glasses containing potassium carbonate (43%), sodium nitrate (59%),
261 and water (100%). Before each measurement, the sample was dried by conditioning at 0 % with silica gel for 96
262 hours to ensure complete drying. Then, they were weighted after 24 hours (Quilez-Molina et al., 2020). The
263 moisture adsorption at each RH condition was calculated following **Equation 6**.

264

265
$$\text{Moisture adsorption at RH (\%)} = \frac{W - W_0}{W_0} \times 100 \text{ (6)}$$

266

267 Where W is the weight after 24 hours at each relative humidity and W_0 is the weight at 0 % RH. These
268 measurements were performed in triplicate.

269

270 For measuring the liquid water absorption, each sample (1.5 cm x 1.5 cm) was weighed after drying in the
271 vacuum oven for 6 hours at 40°C. Then, the foam was placed in 20 ml of distilled water for 10, 20, 45 min, and
272 24 hours. For each time point, the sample was weighed again after removing the excess of water using tissue
273 paper. The results of water adsorption capacity were represented in terms of g liquid water adsorbed/100 g sample
274 at room conditions following **Equation 7**:

275

276
$$\text{Liquid water absorption capability (g/100g of sample)} = \frac{W_t - W_0}{W_t} \times 100 \text{ (7)}$$

277

278 Where W_t is the weight at time t and W_0 is the weight at 0 % RH. These measurements were performed in
279 triplicate.

280

281 Another characteristic is the water-soluble fraction, evaluated following the procedure reported in our
282 previous work (Quilez-Molina, Mazzon, et al., 2022) with slight modifications. The calculation is as follows:
283 the samples were cut in cubes (1.5 cm² x 1.5 cm²), dried in a vacuum oven at 40 °C for 6 hours, and weight (W_0).
284 Then, they were immersed in 20 ml of distilled water for 24 hours, dried again in a vacuum oven for 6 hours at
285 40°C, and weighed (W) to measure the water-soluble fraction. See **Equation 8**.

286
$$\text{Water soluble fraction (\%)} = \frac{W_0 - W}{W_0} \times 100 \text{ (8)}$$

287

288 Where W is the dried weight after the immersion for 24 hours, and W_0 is the weight of the dried sample. These
289 measurements were performed in triplicate.

290

291 *2.3.8 Compression test*

292 Samples were conditioned at 20 °C and 60 % of relative humidity (RH) for 48 hours before the compression test.
293 The deformation rate employed was 2.5 mm/min to a deformation of 70% of the sample weight. The compressive
294 strength was calculated as the maximum load divided by the cross-sectional area of the sample (Duan et al.,
295 2022). The tested dimension is 3.4 x 3.4 cm². The shape recovery (%) was calculated by dividing the recovery
296 height by the height of the sample before the compression test, as reported elsewhere (Kim et al., 2021).

297

298 *2.3.9 Biodegradability test*

299 Tablets of starch and fibers ($\varnothing=13$ mm) were prepared using a Manual Hydraulic Press (Specac) by pressing up
300 to 10 tons. Before testing, a piece of the samples (~ 1 cm x 1 cm) and the tablets were dried for 24 hours at 105
301 °C in an oven Memmert UF55 plus-Universal. Fungal resistance was tested according to the adaptation of
302 European standard EN 350-1 and following the procedure published elsewhere (Can et al., 2023). *Poria* brown
303 rot fungi, *Poria placenta* (Fr.) Lars. & Lombard (Mad-698-R) (Pop) was grown in malt agar media for two weeks
304 in Petri dishes (90 mm diameter). The fungi virulence was tested using samples from *Pinus pinaster* (sapwood)
305 and *Fagus sylvatica* wood. In total, 44 samples (around 10 mm x 10 mm x 5 mm) of various formulations were
306 weighed, sterilized, and put in Petri dishes with fungi. The containers with samples were stored in a climate room
307 at a temperature of 22 °C and 75 % relative humidity for 30 days. After that, all samples were cleaned and then
308 were weighted for moisture content calculations. Then they were dried at a temperature of 70 ± 2 °C, for three
309 days and weighed, and the weight loss was calculated.

310

311 2.3.10 Statistical analysis: Turkey test

312 All the results were reported as mean \pm standard deviation. One-way analysis of variance (ANOVA) and Tukey's
313 test were used to determine the relevance in differences among the mean values at a 0.05 level of significance
314 using Origin 2022 software.

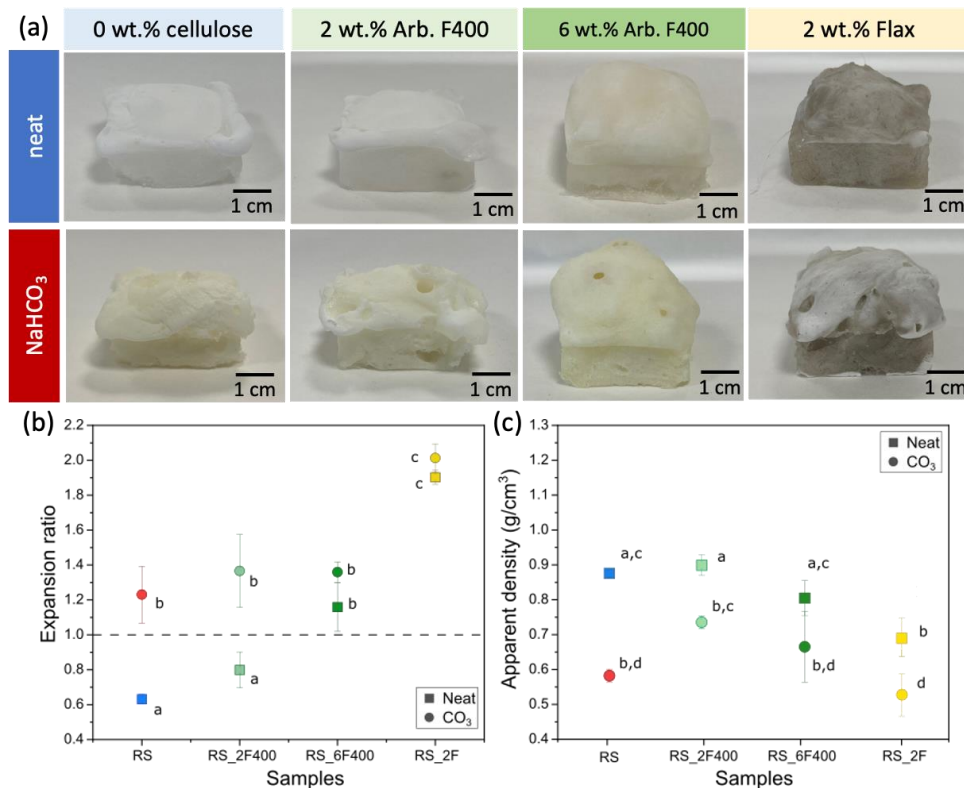
315

316 3. Results and discussion

317 3.1 Analysis of the effect of NaHCO_3 and fillers on the aspect, apparent density, and foamability

318 The inspection of the photographs of the samples reported in **Figure 2 (a)** highlighted that the presence of
319 NaHCO_3 and fibers (type and concentration) had a strong effect on the appearance and expansion capability of
320 the foams. The color of samples was characteristic of the filler used, samples filled with A-F400 were white
321 while F fibers provided a brownish color, see fillers in **Fig. S1 (a-b)**. The blowing agent sodium bicarbonate also
322 induced a colour change towards yellow, which could be associated with a partial dextrinization of starch
323 (Chinnaswamy & Hanna, 1988; Jebalia et al., 2019; Lai et al., 1989). Moreover, this blowing agent generated
324 more visible "super macro holes" or "nodules" on the surface in all the samples. The expansion capability of the
325 samples is represented in **Figure 2 (a)**. Note that the expansion ratio is 1 when the sample does not suffer any
326 volume change. The loss of water during the foaming process and the shrinkage of the starch could result in a
327 final contraction of the sample and the negative value of the RS sample (Liu et al., 2023; S. Peng et al., 2022).
328 It was clearly observed that fibers, long F fibers (3.4 cm) and 6 wt.% of shorter A-F400 microfibers (2 mm), had
329 a positive effect on the foam expansion, reaching values of 2 for samples containing flax fibers. This is because
330 fibers can act as a skeleton during the retraction step, limiting the shrinkage (Liu et al., 2023; S. Peng et al.,
331 2022). As expected, the addition of NaHCO_3 strongly enhanced the starch expansion acting as a blowing agent.
332 The apparent density of samples represented in **Figure 2 (c)** varied from 0.52 to 0.89 g/cm³ depending on the
333 sample. These values were comparable with other starch-cellulose foam composites reported by (Bénézet et al.,
334 2012; Soykeabkaew et al., 2004), or even starch xerogels containing textiles-derived fibers (Négrier et al., 2023).

335 Indeed, some materials qualified for external cushioning packaging, like kraft paper, are around 0.65 g/cm^3 ,
 336 indicating that the materials performed in this study could be suitable for this application (S. Peng et al., 2022).
 337 In general, the density of all starch samples reduced significantly with the addition of NaHCO_3 (represented as
 338 circles in **Figure 2 (c)**). For example, the apparent density of the neat starch sample (RS) decreased from around
 339 0.87 g/cm^3 to 0.58 g/cm^3 for RS_CO_3 . Adding A-F400 did not significantly reduce the apparent density at any
 340 concentration, while foams containing 2 wt.% of F (RS_2F) showed lower density with respect to RS (by 20 %
 341 less).
 342



343 **Figure 2. (a)** The photographs of the samples fabricated in this work. **(b)** The expansion ratio of the foamed
 344 samples, **(c)** The apparent density of water-foamed samples (squares) and water+ NaHCO_3 -foamed samples
 345 (circles). The same letters indicate nonsignificant differences among the results according to Tukey's test ($p <$
 346 0.05).
 347
 348
 349

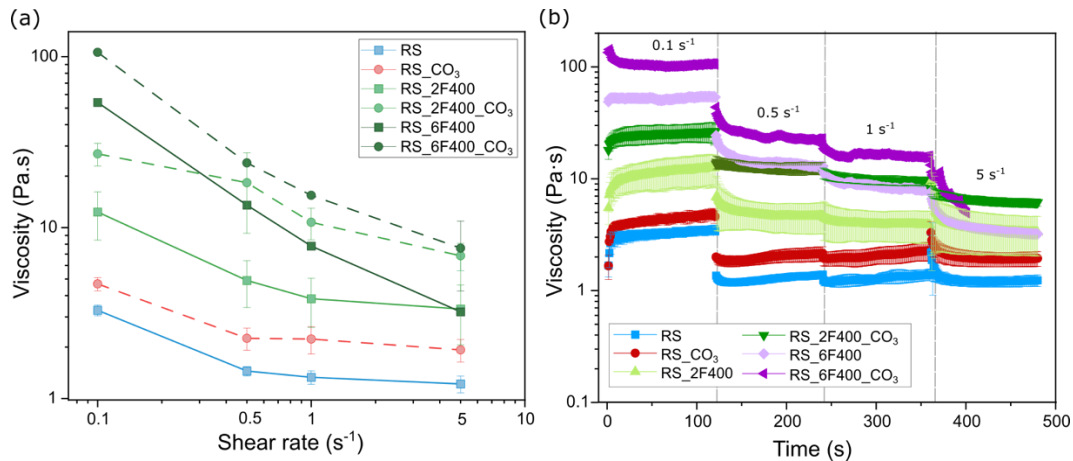
350 3.2 Study of the rheological characteristic of starch composites

351 Fiber-like fillers can usually have two opposite effects on the foaming process of a polymer matrix. On the one
 352 hand, fibers can favour the formation of vapour bubbles during the foaming process acting as a nucleating agent
 353 (Bergel et al., 2021; Duan et al., 2022; Tacha et al., 2023). This occurs due to the presence of micropores or voids
 354 in the polymer-filler interface, which provokes the migration of gas generation from the blowing agent to these

355 regions. This effect usually increases with the concentration and smaller size of fibers (Zhou & Zhang, 2023;
356 Zimmermann et al., 2017). On the other hand, these fillers can promote the increase of apparent viscosity of the
357 initial formulation constituting a “mechanical network” around the cells, inhibiting the pore growth and leading
358 to a denser morphology (Bergel et al., 2021; Négrier et al., 2023; S. Peng et al., 2022; Soykeabkaew et al.,
359 2015). Therefore, the evaluating the influence of each component (i.e., presence of fiber or NaHCO₃, type of
360 fiber) on the overall viscosity was analyzed in terms of the rheological behaviour of the starch suspension (before
361 the MW irradiation). **Figure 3 (a)** exhibits the values of viscosity at different shear rates for each sample. Results
362 revealed that the viscosity globally decreased with increasing the shear rate, indicating a shear thinning behaviour
363 of the samples. As expected, the viscosity increased with the content of fiber. The higher viscosities at the low
364 shear rate observed when A-F400 fiber was added could be interpreted as a consequence of the apparition of an
365 H-bonding network between the cellulose fiber and the starch, as already reported by (X. W. Peng et al., 2011;
366 Xie et al., 2013). However, interestingly, the shear thinning behaviour was more pronounced when the
367 concentration of fibers increased (see curves RS_2F400 and RS_6F400). The decrement of viscosity when the
368 shear rate increased could be related to the disruption of the linkages between the starch particles and fibers, as
369 well as with the alignment of fiber along the flow (Greene & Wilkes, 1995; Ou et al., 2014). The alignment of
370 the fibers is an effect commonly observed in fiber-filled polymers, such as polypropylene, polycarbonate, or
371 nylon 6/6 (Greene & Wilkes, 1995). However, this decrement was less significant in samples filled with
372 NaHCO₃, regardless of the concentration of fiber. This could be associated with an increment of H-bonding
373 interaction between the fibers and starch, due to the pulping effect of the NaHCO₃, which hampered the
374 alignment of the fibers (X. W. Peng et al., 2011; L. Zhang et al., 2021). The higher viscosity observed in starch
375 samples loaded with fibers could have provided a good dimensional stability to foams preventing the shrinkage
376 after the foam expansion, see **Figure 2(b)**.

377 **Figure 3 (b)** displays the viscosity versus time at the different shear rates applied. All samples exhibited a
378 complex behavior, displaying an unstable viscosity after 2 min of shear (e.g., shear rates 0.5 and 1 s⁻¹ for RS and
379 RS_CO₃ systems). This instability at a constant shear rate was probably due to the thixotropic behavior of the
380 suspensions, which was not surprising at such particle concentration (starch and fiber beyond 50 wt.%) (Wang
381 et al., 2022). It is important to note that the high length of F fibers hindered the measurement of viscosity for
382 this set of samples, and the noisy signal obtained at 5 s⁻¹ for RS_6F400_CO₃ was associated with the apparition
383 of strong heterogeneities in the material, ejected in part from the geometry.

384

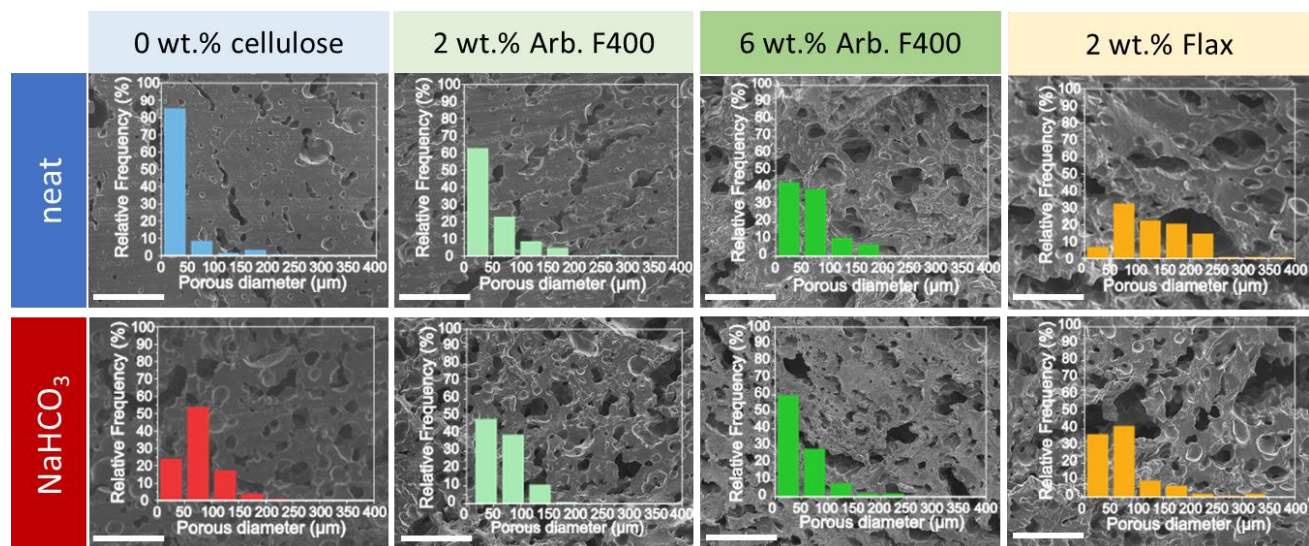


385
 386 **Figure 3. (a)** The flow curves of the pre-foaming samples, viscosity vs shear rate. The values of viscosities
 387 represented were taken at the end of the application of a given shear rate. **(b)** Viscosity vs time for each shear
 388 rate 0.1-5 s⁻¹. Note that these values may not reflect the steady-state viscosities.

390 3.3 Inner morphology of the foam composite

391 **Figure 4** displays the cross-section images of all the samples with the corresponding pore's diameter diagrams
 392 (inset figure). In all cases, the foams displayed very non-uniform porosity, with a pores size distribution ranging
 393 from 1 μm to 400 μm , as a result of the presence of different porogenic molecules and blowing agents involved
 394 in the foaming process (i.e., water and CO₂). All micrographs displayed cracks and holes that suggested a highly
 395 interconnected cellular structure, as observed in similar works (Bergel et al., 2021; Lopez-Gil et al., 2015).
 396 The values of cell density (cell/cm³ x 10⁶), average cell size (μm), and porosity are reported in **Table 2**. The
 397 results of the cell density (cell/cm³ x 10⁶) and porosity revealed the positive effect of the NaHCO₃ and fibers on
 398 increasing the number of pores on the starch matrix, acting as a blowing and nucleating agent, respectively. In
 399 comparison, the results of cell density were slightly greater than those presented in polycarbonate foams filled
 400 with long carbon fiber and short glass fiber (Zhou & Zhang, 2023). The lower apparent density of cellulosic-
 401 fiber composites was also associated with the increment of the size of the pores observed in these samples.
 402 Especially in samples filled with F, up to three times values displayed by neat foams for RS_2F sample, 39 μm
 403 in RS against 97 μm in RS_2F, denoting the positive effect of the length of the fiber on the pore growing. Peng
 404 S et al., (S. Peng et al., 2022) reported that long microfibers (> 1mm) enhance the formation of bigger bubbles
 405 due to the better capability of conducting the stress after the bubble disruption and retraction of the starch.
 406 Zimmermann M. et al., (Zimmermann et al., 2017) reported the high importance of the aggregation tendency of
 407 fibers, which increases with content and length, promoting larger cells. This occurs because the gas from the
 408 blowing agent tends to migrate to the least resistant region and propagates its growth from this point. Therefore,
 409 the notable reduction of pore size when these samples were treated with NaHCO₃ could indicate a better
 410 dispersion of the fibers through the matrix.

411 As explained previously, the viscosity of the batter is also highly important for the foaming process because it
 412 limits the expansion of the bubble (Bergel et al., 2021; S. Peng et al., 2022). A major intermolecular interaction
 413 between the fibers and starch with the pulping effect of NaHCO_3 , which resulted in an increment of hydroxyl
 414 groups available, resulted in an increment of the viscosity (see **Figure 3**) (Liu et al., 2023). The effect of the
 415 pulping treatment on the cellulosic fibers was evidenced with microscopy, thermogravimetric analysis, and
 416 infrared spectroscopy of **Figures S4 and S5** in Supporting information. Fibers were easily appreciable and
 417 appeared well impregnated in the starch matrix in the micrographs reported in **Figure S6** of Supporting
 418 information, evidencing the good compatibility between the two components and the eventual attaching of the
 419 starch after retraction (Lopez-Gil et al., 2015; Prachayawarakorn et al., 2011). It's worth noticing that the thermal
 420 degradation of fibers started around 200 °C, revealing that the temperature could damage the fiber features, such
 421 as the extrusion with polymers with higher processing temperatures, like polypropylene (PP) and polylactic acid
 422 (PLA) (Peltola et al., 2014; Völtz et al., 2023; Wei et al., 2023). Moreover, extrusion can lead to the breakage of
 423 long fibers or degrading, while microwave ensures the preservation of the long fibers' morphology after the
 424 processing (Peltola et al., 2014; Rodríguez-Fabià et al., 2023; Zhou & Zhang, 2023). Finally, as observed in other
 425 starch foams loaded with fibers processed through similar methods (Lopez-Gil et al., 2015; Rodríguez-Fabià et
 426 al., 2023), fibers were not oriented inside the matrix.
 427



428
 429 **Figure 4.** The cross-section SEM images and histograms of the porous size distribution of all the samples.
 430

| Sample | Average cell size (μm) | Porosity (%) | Cell density (cell/cm ³ · 10 ⁶) |
|--------------------|------------------------|--------------|--|
| RS | 39 ± 36 | 41 | 1.4 |
| RS_CO ₃ | 76 ± 39 | 61 | 17.4 |
| RS_2F400 | 55 ± 45 | 40 | 3.0 |

| | | | |
|--------------------------|---------|----|------|
| RS_2F400_CO ₃ | 71 ± 42 | 51 | 10.9 |
| RS_6F400 | 66 ± 43 | 46 | 3.2 |
| RS_6F400_CO ₃ | 54 ± 42 | 55 | 10.6 |
| RS_2F | 97 ± 56 | 54 | 3.6 |
| RS_2F_CO ₃ | 79 ± 63 | 65 | 9.6 |

431 **Table 2.** Values of porosity, cell density, and average cell size of the starch foam composites.

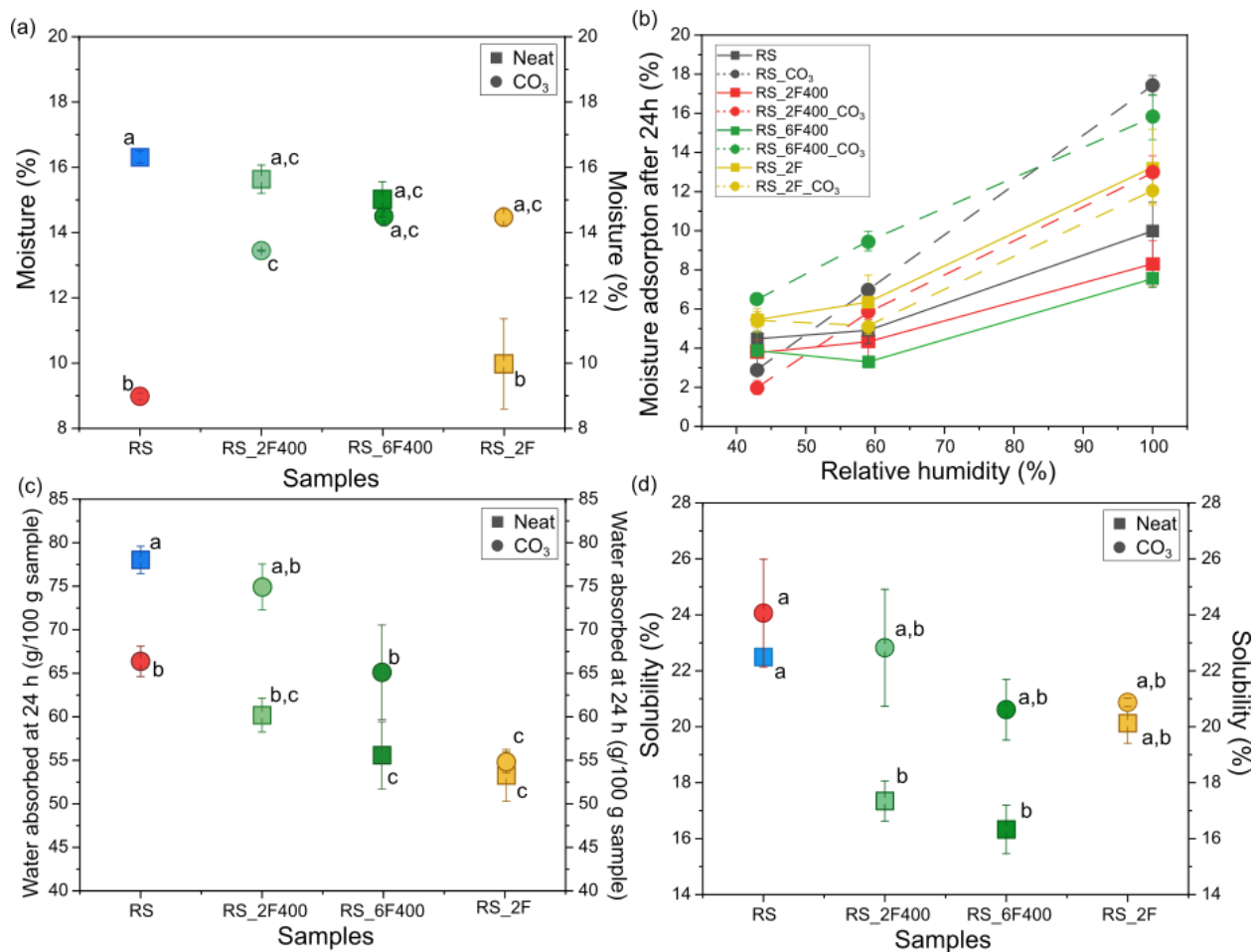
432

433 3.4 Water resistance properties

434 The results of the moisture content of neat and composite foams are represented in Figure 5(a). Neat starch foam
 435 exhibited around 17% moisture content, slightly superior to other starch composites reported in the literature
 436 (Bergel et al., 2021; Quilez-Molina et al., 2023). The addition of fibers reduced the moisture content in starch
 437 foams, likely due to the formation of hydrogen bonds between the hydrophilic filler and the starch matrix,
 438 preventing the interaction between the OH of starch molecules with water moisture (Bergel et al., 2021; Quilez-
 439 Molina, Chandra Paul, et al., 2022). The bleaching effect of NaHCO₃ resulted in an increment of moisture
 440 sensitivity of cellulosic-starch composites, especially in flax fibers (RS_2F_CO₃), see SEM images and infrared
 441 spectra **Figure S5(f)** of Supporting information. The moisture adsorption of the samples after exposure for 24
 442 hours to different humidity environmental conditions is represented in **Figure 5 (b)**. As expected, the moisture
 443 adsorption increased with the relative moisture environment, although a decrease in adsorption was observed
 444 with the incorporation of filler. The increment of moisture adsorption in samples treated with NaHCO₃ was
 445 linked to the superior porosity, which contributed increasing the available surface for water interaction (Bergel
 446 et al., 2021).

447 Noticeably, the starch foams loaded with 6 wt.% of A-F400 (RS_6F400) displayed a moisture adsorption value
 448 of 4 % after being exposed for 24 hours to 100 % humidity, which highlights the greater stability of the composite
 449 to outdoor applications. The values of the water adsorption (g water/ 100 g of sample) of the foams after 24
 450 hours are represented in **Figure 5 (c)**. These results showed the remarkable positive effect of the fibers in
 451 improving the water resistance in samples, which increased with the fiber content and especially with F. As
 452 observed above, these results were associated with the interaction between cellulose and starch matrix, and with
 453 the hydrophobic nature of flax (Bergel et al., 2021; Prabhakar et al., 2017; Prachayawarakorn et al., 2011). The
 454 values obtained in samples without NaHCO₃ (below 60 g/100 g sample) were quite below with respect to other
 455 thermoplastic starch foams containing 1, 3, and 5 wt.% of cotton fibers, which showed 68-80 g of water/100 g
 456 solid (Bergel et al., 2021). Interestingly, these results were comparable with extruded starch-based foams
 457 combined with a petroleum-derived polymer (polyvinyl alcohol, PVA) with different hydrolysis degrees (Liu et
 458 al., 2023). As observed in **Fig. S7** of Supporting information, these differences are remarkable from the first 10
 459 min of water adsorption, which reached a maximum of 55 g water/100g sample for RS_6F400_CO₃, and which
 460 was entirely accomplished within the first hour. This effect was associated with the sample open-cell porosity,

461 which facilitated the entrance of water permeation and diffusion through microstructure (Bergel et al., 2021).
 462 **Figure 5 (d)** displays the values of the water solubility fraction of samples after 24 hours of water immersion.
 463 As a general rule, the addition of fibers strengthened the water resistance of the foam composites by reducing
 464 the water solubility fraction by hydrogen bond interaction. The higher solubility of samples treated with NaHCO_3
 465 was associated with the LMW-starch molecules due to the starch dextrinization, which present water solubility
 466 (Bergel et al., 2021; Quilez-Molina et al., 2023).
 467 In summary, results showed that the treatment with NaHCO_3 had a negative effect on the water sensitivity
 468 properties of the cellulosic-starch composite foams, while the filler improved the resistance of starch by creating
 469 a hydrogen network with the matrix. Overall, the sample RS_6F400 was shown to provide the best water-
 470 resistance features, especially in terms of water adsorption and solubility.
 471



472
 473 **Figure 5.** The values of (a) moisture (b) water adsorbed after 24 hours in fixed RH%, (b) liquid water adsorbed
 474 after immersion for 24h and (c) water-soluble fraction of all the neat samples, represented as squares, and
 475 samples treated with NaHCO_3 , represented as circles. The same letters indicate nonsignificant differences among
 476 the results according to Tukey's test ($p < 0.05$).
 477

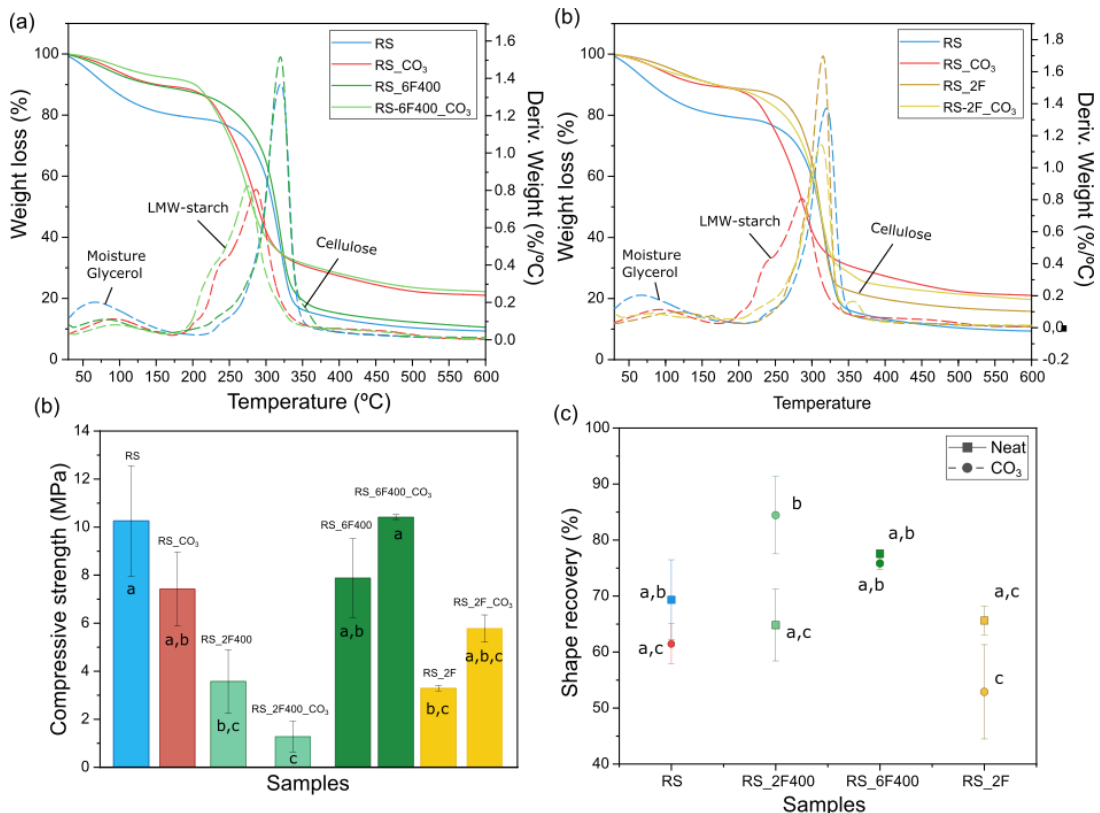
478

479 3.5 Thermal and mechanical properties

480 In **Figures 6 (a-b)**, the thermal degradation curve of the neat starch (coloured in blue) was shown to degrade in
481 two main steps. The first degradation step occurred below 200°C associated with the volatilization of moisture
482 and glycerol, while the main mass loss step (60%), associated with the decomposition of the starch, occurred in
483 a range of 250-360 °C, with the maximum decomposition rate at 320 °C (Prabhakar et al., 2017). **Figure 6 (a)**
484 shows that the addition of A-F400 in 6 wt.% did not modify the thermal degradation of starch (320 °C), however,
485 the thermal profiles exhibited an important decrement of moisture loss, which indicated the cellulosic fibers
486 reduced the absorption of moisture. The low amount of moisture is very important in terms of material stability
487 and applicability (Liu et al., 2023; Soykeabkaew et al., 2015). Noticeably, the effect of the treatment with
488 NaHCO₃ was easily observed in the thermal profile of RS_CO₃ and RS_6F400_CO₃ samples. Contrary to the
489 neat samples, the thermal degradation occurred in two steps at lower temperatures: a new peak at about 237 °C,
490 with a mass loss of 12%, and the main degradation peak downshifted to 240°C (about 10 °C less). These thermal
491 patterns were associated with the presence of low-molecular-weight (LMW) starch molecules (i.e., dextrans) that
492 decompose at a lower temperature due to the basic hydrolytic conditions in presence of NaHCO₃ (pH ~ 8.5),
493 coupled with the microwave irradiation, (F. Chen et al., 2019; Quilez-Molina et al., 2023; Zuo et al., 2014). The
494 thermal curves of samples containing F fibers displayed in **Figure 6 (b)** revealed that F slightly reduced the
495 thermal resistance of the starch, exhibiting the maximum degradation peak at 315 °C, 5 °C below the neat RS
496 sample. The content of hemicellulose, which has weaker thermal properties, led to composites with lower
497 thermal resistance (Merino & Athanassiou, 2023; Quilez-Molina, Chandra Paul, et al., 2022). Interestingly, the
498 peak related to the LWM-starch is rather visible in RS_2F_CO₃, which might suggest that F fibers protected
499 starch from degradation. Similar to A-F400 fibers, the addition of F fibers reduced the moisture content on starch
500 composites. The increment of residual char was associated with the Na₂CO₃ resulting from the thermal
501 decomposition of NaHCO₃, as observed with other composites containing inorganic additives (Z. X. Zhang et
502 al., 2012).

503 In general, the chemical composition of rice starch, based on low content of amylose biopolymer (~25%) and
504 rich in amylopectin (~75%), makes this kind of starch quite friable and brittle (Prachayawarakorn et al., 2011).
505 The addition of cellulosic fibers as reinforcement has been a widely easy method employed to improve this
506 property (Peltola et al., 2014; Rodríguez-Fabià et al., 2023). The compression curve of the RS_2F400, selected
507 as a representative example, is displayed in **Figure S8**. The compression stress-strain curve showed the typical
508 profile of hard foams, which consisted of a first linear elasticity region (up to strain of 5-10%), followed by a
509 slight plateau of deformation, and a final zone where the collapse of the closed cell structure and foam
510 densification occurs (Kim et al., 2021; Miranda-Valdez et al., 2023). However, the profile of the compression
511 stress-strain curves strongly depends on the polymeric cell structure. Generally, in high-density polymeric foams,
512 such as the materials presented in this work, the stress gradually increases beyond the elastic zone up to the cell
513 collapse (Kim et al., 2021). Similar compression curves have been also observed in other starch-based composite

514 foams loaded with sisal fibers (5 mm) (Ji et al., 2021). **Figure 6 (a)** displays the compressive strength of the
 515 samples with 70 % compression. Results showed that NaHCO₃ contributed to the reduction of foam rigidity in
 516 RS_CO₃ and RS_2F400_CO₃, in comparison with untreated samples. However, the mechanical strength was
 517 improved in RS_6F400_CO₃ and RS_2F_CO₃. This result was associated with the effect of NaHCO₃ in
 518 modifying the cell size, smaller cell size is related to better mechanical properties (Kim et al., 2021; Zhou &
 519 Zhang, 2023). For the latter samples, NaHCO₃ improved the fibers' dispersion after the pulping with NaHCO₃,
 520 which reduced the formation of agglomerates and increased the hydrogen bonding network (Bergel et al., 2021;
 521 Bernaoui et al., 2022; Rodríguez-Fabià et al., 2023). Therefore, the mechanical properties of starch foams were
 522 mainly subjected to their microstructure (i.e., porosity) and fiber dispersion.
 523 The results of compressive strength obtained for some of these composites greatly exceeded, up to 3 times, the
 524 values exhibited in starch foams reinforced with sisal fiber of 1 mm, 5 mm, and 10 mm loaded in 40% (~ 2
 525 MPa) (S. Peng et al., 2022). The shape recovery (%) is represented in **Figure 6 (b)**. These results highlighted the
 526 capability of the samples to recover the original shape after the compression test, which is strongly dependent
 527 on the friability of the cells (Kim et al., 2021). Overall, all samples showed relatively good recovery properties
 528 after compressions up to 70% of the original height, showing a minimum of 52 % for RS_2F_CO₃ and a
 529 maximum of 84 % for RS_2F400_CO₃. Overall, samples filled with 6 wt.% of A-F400 (with or without
 530 NaHCO₃) displayed better shape recovery, which indicated that these fiber's efficiency prevented the collapse of
 531 the cells at high compression loadings. Interestingly, the plasticizing effect of water could have positively
 532 contributed to the great value of recovery obtained in these foams (Mali et al., 2010; Soykeabkaew et al., 2004).



533

534 **Figure 6.** TG and DGT curves and thermal values of RS samples filled with **(a)** A-F400 and **(b)** F fibers. **(c)** The
535 compressive strength values for each sample. **(d)** The shape recovery values. The same letters indicate
536 nonsignificant differences among the results according to Tukey's test ($p < 0.05$).

537

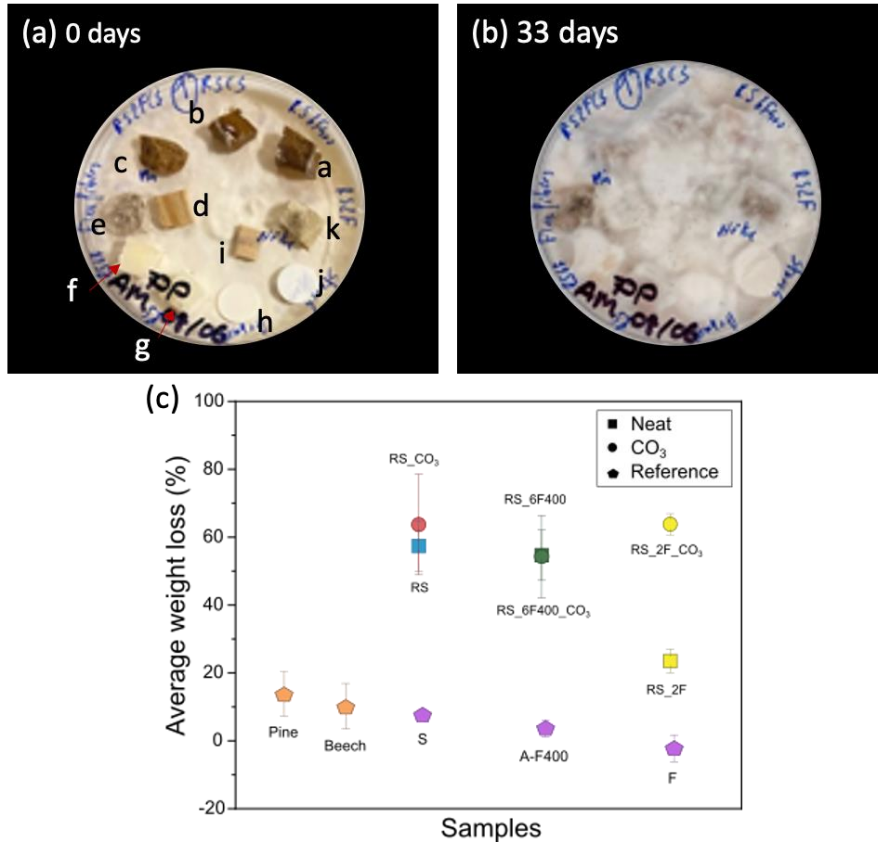
538 3.6 Biodegradation

539 Evaluating the biodegradability of samples is highly important for the application of these eco-friendly
540 composites in the environment. A biodegradation test was carried out with the brown-rot fungus *Poria Placenta*,
541 ubiquitously found in nature, which degrades cellulose (preferentially) and lignin (Can et al., 2023).

542 The biodegradability of the dried porous samples ($1 \times 1 \times 0.5 \text{ cm}^3$) was tested and compared with dried tablets of
543 neat dry sintered starch-dense powder, A-F400, and F, as well as wooden pieces of pine and beech ($1 \times 1 \times 0.5$
544 cm^3), used as references. Each replicate of the sample and reference was placed in the same Petri dish with the
545 same sample's repartition, see the photograph of **Figure 7 (a)**. 4 Petri dishes of malt-agar and inoculated fungus
546 were incubated ($25 \text{ }^\circ\text{C}$, 70 % RH) for 33 days. As observed in **Figures 7 (a-b)**, at the end of the experiment the
547 colony of fungi greatly expanded to completely cover the samples. During this process, the fungi grew on the
548 surface of the foam, decomposing and fragmenting the sample to obtain the nutrients (Can et al., 2023; J. Zhang
549 et al., 2022). The results of the biodegradability test are displayed in **Figure 7 (c)**. The first global observation
550 is that a period of 33 days was quite enough to degrade most of the starch-based foams/composites to a large
551 extent ($> 50 \text{ wt.}\%$), overcoming greatly the degradation of the wooden pieces of pine and beech, and the neat-
552 sintered reference tablets. This high biodegradation rate was comparable with the degradation in the soil of other
553 starch foams filled with fibers, such as the cassava starch foams filled with 10 wt.% of sugarcane fibers reported
554 by (Ketkaew et al., 2018). Generally, the capability of the microbe to degrade the matter depends on the nature
555 of the material (hydrophilicity, and crystallinity), the humidity conditions, and the compacity of the material
556 (porosity) (Prabhakar et al., 2017). However, it can be assumed that the effect of porosity was predominant,
557 while the influence of starch material was the second trigger (comparing porous starch to dense starch). **Table**
558 **S1** relates the highest mass losses to the highest porosities; the most porous ($> 40\%$) being the most degraded ($>$
559 60%). Note that densified starch or densified cellulose fibers needed a longer time to degrade.

560 In the SEM pictures of the biodegraded samples reported in **Fig. S9 (a-d)** of Supporting information, the
561 mycelium and fungus elements were easily distinguished on all the samples. The ubiquitous expansion of the
562 mycelium overall the surface underlined the good adhesion and affinity with the samples. Moreover, the
563 apparition of holes randomly distributed on the samples (marked with red arrows in **Fig. S10**), noted the
564 degradation of the organic matter (Can et al., 2023). The lack of these holes on wood pieces might confirm the
565 lower degradation rate in comparison with starch-based samples.

566



567
 568 **Figure 7.** The photograph of the samples **(a)** at the beginning and **(b)** at the end of the biodegradability test. The
 569 samples were marked as a: RS_6F400_CO₃, b: RS_CO₃, c: RS_2F_CO₃, d: pine, e: flax fibers, f: RS_6F400, g:
 570 RS, h: A-F400 fibers, i: beech, j: starch powder, and k: RS_2F. **(c)** The average weight loss of specimens after
 571 33 days of experiment.

572
 573

574 3.7 Sustainability study: Greenhouse gas (GHG) emissions

575 As introduced before, this project is conceived with the aim of employing fiber waste from the textile industry
 576 as a cellulosic filler. Therefore, separated cotton clothing fibers, in a size around 2 mm and without dyes, (such
 577 as commercial A-F400 fibers) were considered as the filler to obtain the sample that presented the best properties,
 578 RS_6F400. Moreover, it will only be considered the GHG generated during the production and treatment of the
 579 reagents, as well as during the sample fabrication.

580 According to the study reported by Espinoza-Pérez L., et al., (Espinoza Pérez et al., 2022), the treatment of
 581 recycling textile fibers generated about 1142.12 kg CO_{2eq}/ton of fiber. Therefore, for this formulation, the fiber
 582 processing corresponded to 55 kgCO_{2eq} per ton of foam composite. Moreover, the GHG emissions associated
 583 with the extraction processing of the crop to obtain the starch polymer were around 105-150 kg CO_{2eq}/t, which
 584 can vary with the crop and producing country (Tran et al., 2015). It's important to consider that the values of net
 585 GHG emissions for other non-biodegradable petroleum-based plastics like polypropylene (PP) and low-density

586 polyethylene (LDPE) are close to 2000 kg CO_{2eq}/t in both polymers (Broeren et al., 2017; Pang et al., 2014).
 587 This corresponds to a total of 81 kgCO_{2eq} per ton of RS_6F400 produced. The plasticizers usually have GHG
 588 emissions of 1950 kg CO_{2eq}/ton (Broeren et al., 2016; Pang et al., 2014), which corresponds to 390 kgCO_{2eq} per
 589 ton of the present formulation. The values of carbon intensity (CI) of electricity consumed at low voltage found
 590 elsewhere (Scarlat et al., 2022), corresponded to 0.98 gCO₂/kWh in France in 2019. Considering this data, the
 591 MW processing produced 0.81 kgCO_{2eq} per ton of material fabricated. The sum of all these factors resulted in a
 592 total of around 526 kgCO_{2eq} per ton of the RS_6F400 foam. Interestingly, the GHG emitted for the material
 593 production are comparable with textile fibers (without recycling process) combined with cheap petroleum-based
 594 polymer PP through extrusion reported by Völtz L. *et al.*, (Völtz et al., 2023), or better than other polymer
 595 composites reported in **Table 3**. Moreover, it's important to highlight the potential environmental benefits, in
 596 terms of biobased feedstock and excellent biodegradability in natural conditions (see biodegradability test). The
 597 latter is greatly interesting for avoiding additional costs related to waste management or recycling, but also for
 598 reducing environmental impact due to the calcination of plastics. For fibers, the calcination of textiles in landfills
 599 corresponds to around 0.423 kg CO_{2eq}/kg, while plastic wastes generate around 5.1 tons of CO₂ every year
 600 (Correa et al., 2019; Espinoza Pérez et al., 2022). To conclude, it's worth noticing that the plasticizer was the
 601 component that contributed more to the GHG emission, which underlined the importance of searching for new
 602 plasticizers for reducing the carbon footprint in future works.
 603

| Material | Filler (wt.%) | Fabrication method | kgCO_{2eq}/ton composite | Reference |
|-------------------------------------|---|-------------------------------|---|---------------------------|
| Starch foamed composites | 6 wt.% Arbocell® A-F400 fibers (2 mm) | Microwave irradiation | 526 | This work |
| PP composites | 20 wt.% Talc | Extrusion + Thermoforming | 4430 | (Pang et al., 2014) |
| PLA/ TPS | - | Extrusion + Thermoforming | 1000 | (Broeren et al., 2017) |
| PP composites | 30 wt.% cotton fiber | Extrusion + Thermoforming | 555 | (Völtz et al., 2023) |
| PP composites | 30 wt.% glass fiber | Extrusion + Thermoforming | ~6700 | (Boland et al., 2016) |
| PP composites | 40 wt.% kenaf fiber | Extrusion + Thermoforming | ~5300 | (Boland et al., 2016) |

604 **Table 3.** Values of GHG emissions for different polymer composites. Abbreviations: PLA= polylactic acid;
 605 TPS=Thermoplastic starch; PP=polypropylene. Note that the values calculated were approximative. Some costs,

606 such as the raw material transportation or use phase, were not considered in this work. This could have influenced
607 the difference in emissions concerning other works whose aim was only the study of the life cycle assessment
608 of the composites.

609
610

611 **4. Conclusion**

612 “All polysaccharide” composite foams from cellulosic fibers resources, with lower density, good water, and
613 mechanical resistance, and excellent degradability through a sustainable and low-cost process were successfully
614 achieved. Sodium bicarbonate, with a double role as a blowing and pulping agent, was shown to be critical to
615 defining the final properties of the starch foams by reducing the apparent density of foams, but also by improving
616 the dispersion and interaction with the matrix (i.e., removing non-cellulosic carbohydrates). As a result, the
617 mechanical properties of the fiber’s composites pulped with NaHCO₃ showed better thermal and mechanical
618 resistance, the latter was associated with the increasing hydrogen bond network and reduction of fibers’
619 agglomerates, which otherwise promoted bigger pores with poorer mechanical features. However, the higher
620 porosity reached with NaHCO₃ was shown to have a negative effect on the water resistance properties of foams.
621 Overall, the sample RS_6F400 (i.e., 6wt% pure cellulose fibers) showed the best properties in terms of low
622 density, mechanical, thermal, and water resistance properties, as well as excellent biodegradability. However,
623 the pulping treatment remarkably improved the properties of starch composites containing raw textile flax fibers,
624 which suggests that this treatment could be employed for fabricating sustainable composites with fibers that
625 present similar chemical features.

626 In conclusion, most starch foams containing cellulosic fibers exhibited excellent biodegradability in contact with
627 the fungus *Poria Placenta*, losing more than 50 % of the initial weight. In addition to their good functionalities,
628 these composites exhibited a better environmental performance than analogous systems. The foams can be
629 designed to give a second life cycle to industrial waste (textile fibers), as assessed by a calculation of low GHG
630 emissions.

631
632

633 **Acknowledgements**

634 The authors gratefully acknowledge Jean-Marc Tallon, from the Department of Science et Genie des Matériaux
635 (IUT Bordeaux) for the technical assistance in SEM observations, as well as Jean-Eudes Maigret, from
636 Laboratory BIA at INRAE Nantes for measurement of the amylose content of rice starch by a calorimetry
637 analysis. Finally, we thank the Spanish Ministry of Universities and the Next Generation EU-Recovery for
638 funding the post-doctoral grant “Margarita Salas” of A. Q.

639

640 **References**

641 Adu, C., Jolly, M., & Thakur, V. K. (2018). Exploring new horizons for paper recycling: A review of
642 biomaterials and biorefinery feedstocks derived from wastepaper. In *Current Opinion in*
643 *Green and Sustainable Chemistry* (Vol. 13, pp. 21–26). Elsevier B.V.
644 <https://doi.org/10.1016/j.cogsc.2018.03.003>

645 Alam, M. N., & Christopher, L. P. (2017). A novel, cost-effective and eco-friendly method for
646 preparation of textile fibers from cellulosic pulps. *Carbohydrate Polymers*, *173*, 253–258.
647 <https://doi.org/10.1016/j.carbpol.2017.06.005>

648 Bénézet, J. C., Stanojlovic-Davidovic, A., Bergeret, A., Ferry, L., & Crespy, A. (2012). Mechanical
649 and physical properties of expanded starch, reinforced by natural fibres. *Industrial Crops*
650 *and Products*, *37*(1), 435–440. <https://doi.org/10.1016/j.indcrop.2011.07.001>

651 Bergel, B. F., Araujo, L. L., & Santana, R. M. C. (2021). Effects of the addition of cotton fibers and
652 cotton microfibers on the structure and mechanical properties of starch foams made from
653 potato starch. *Carbohydrate Polymer Technologies and Applications*, *2*.
654 <https://doi.org/10.1016/j.carpta.2021.100167>

655 Bernaoui, A., Lebrun, G., & Ruiz, E. (2022). High performance natural fiber composites from mat
656 and UD flax reinforcements backed with a mat Binder: a study of mat fiber surface
657 fibrillation. *Composites Part A: Applied Science and Manufacturing*, *160*, 107064.

658 Boland, C. S., De Kleine, R., Keoleian, G. A., Lee, E. C., Kim, H. C., & Wallington, T. J. (2016). Life
659 Cycle Impacts of Natural Fiber Composites for Automotive Applications: Effects of
660 Renewable Energy Content and Lightweighting. *Journal of Industrial Ecology*, *20*(1), 179–
661 189. <https://doi.org/10.1111/jiec.12286>

662 Broeren, M. L. M., Kuling, L., Worrell, E., & Shen, L. (2017). Environmental impact assessment of
663 six starch plastics focusing on wastewater-derived starch and additives. *Resources,*
664 *Conservation and Recycling*, *127*, 246–255.
665 <https://doi.org/10.1016/j.resconrec.2017.09.001>

666 Broeren, M. L. M., Molenveld, K., van den Oever, M. J. A., Patel, M. K., Worrell, E., & Shen, L.
667 (2016). Early-stage sustainability assessment to assist with material selection: a case study
668 for biobased printer panels. *Journal of Cleaner Production*, *135*, 30–41.
669 <https://doi.org/10.1016/j.jclepro.2016.05.159>

670 Can, A., Tomak, E. D., Ermeydan, M. A., & Aykanat, O. (2023). Synergic effect of basalt/wood
671 fiber reinforced polylactic acid hybrid biocomposites against fungal decay. *European*
672 *Polymer Journal*, 112246.

673 Chen, F., Xie, F., Liu, P., & Chen, P. (2019). Structure, thermal stability and suspension rheological
674 properties of alcohol–alkali-treated waxy rice starch. *International Journal of Biological*
675 *Macromolecules*, *134*, 397–404. <https://doi.org/10.1016/j.ijbiomac.2019.05.009>

676 Chen, H., Yu, Y., Zhong, T., Wu, Y., Li, Y., Wu, Z., & Fei, B. (2017). Effect of alkali treatment on
677 microstructure and mechanical properties of individual bamboo fibers. *Cellulose*, *24*(1),
678 333–347. <https://doi.org/10.1007/s10570-016-1116-6>

679 Chinnaswamy, R., & Hanna, M. A. (1988). Expansion, Color and Shear Strength Properties of
680 Com Starches Extrusion-Cooked with Urea and Salts. *Starch - Stärke*, *40*(5), 186–190.
681 <https://doi.org/10.1002/star.19880400507>

682 Correa, J. P., Montalvo-Navarrete, J. M., & Hidalgo-Salazar, M. A. (2019). Carbon footprint
683 considerations for biocomposite materials for sustainable products: A review. In *Journal of*

684 *Cleaner Production* (Vol. 208, pp. 785–794). Elsevier Ltd.
685 <https://doi.org/10.1016/j.jclepro.2018.10.099>

686 Dong, Z., Li, N., Chu, T., Ding, J., Zhang, J., & Dong, A. (2022). High-Quality Natural Fibers from
687 Cotton Stalk Bark via Limited Alkali Penetration and Simultaneous Accelerated Temperature
688 Rise. *Materials*, *15*(2). <https://doi.org/10.3390/ma15020422>

689 Duan, Q., Zhu, Z., Chen, Y., Liu, H., Yang, M., Chen, L., & Yu, L. (2022). Starch-Based Foams
690 Nucleated and Reinforced by Polysaccharide-Based Crystals. *ACS Sustainable Chemistry and*
691 *Engineering*, *10*(6), 2169–2179. <https://doi.org/10.1021/acssuschemeng.1c07738>

692 Espinoza Pérez, L. A., Espinoza Pérez, A. T., & Vásquez, Ó. C. (2022). Exploring an alternative to
693 the Chilean textile waste: A carbon footprint assessment of a textile recycling process.
694 *Science of the Total Environment*, *830*. <https://doi.org/10.1016/j.scitotenv.2022.154542>

695 Foulk, J. A., Chao, W. Y., Akin, D. E., Dodd, R. B., & Layton, P. A. (2006). Analysis of flax and cotton
696 fiber fabric blends and recycled polyethylene composites. *Journal of Polymers and the*
697 *Environment*, *14*(1), 15–25. <https://doi.org/10.1007/s10924-005-8703-1>

698 Georges, A., Lacoste, C., & Damien, E. (2018). Effect of formulation and process on the
699 extrudability of starch-based foam cushions. *Industrial Crops and Products*, *115*, 306–314.
700 <https://doi.org/10.1016/j.indcrop.2018.02.001>

701 Gimeno, E., Moraru, C. I., & Kokini, J. L. (2004). Effect of Xanthan Gum and CMC on the Structure
702 and Texture of Corn Flour Pellets Expanded by Microwave Heating. *Cereal Chemistry*, *81*(1),
703 100–107. <https://doi.org/10.1094/CCHEM.2004.81.1.100>

704 Greene, J. P., & Wilkes, J. O. (1995). Steady-State and dynamic properties of concentrated fiber-
705 filled thermoplastics. *Polymer Engineering & Science*, *35*(21), 1670–1681.
706 <https://doi.org/10.1002/pen.760352103>

707 Jebalia, I., Maigret, J. E., Réguerre, A. L., Novales, B., Guessasma, S., Lourdin, D., Della Valle, G.,
708 & Kristiawan, M. (2019). Morphology and mechanical behaviour of pea-based starch-
709 protein composites obtained by extrusion. *Carbohydrate Polymers*, *223*.
710 <https://doi.org/10.1016/j.carbpol.2019.115086>

711 Ji, M., Li, F., Li, J., Li, J., Zhang, C., Sun, K., & Guo, Z. (2021). Enhanced mechanical properties,
712 water resistance, thermal stability, and biodegradation of the starch-sisal fibre composites
713 with various fillers. *Materials and Design*, *198*.
714 <https://doi.org/10.1016/j.matdes.2020.109373>

715 Juanga-Labayen, J. P., Labayen, I. V., & Yuan, Q. (2022). A Review on Textile Recycling Practices
716 and Challenges. *Textiles*, *2*(1), 174–188. <https://doi.org/10.3390/textiles2010010>

717 Ketkaew, S., Kasemsiri, P., Hiziroglu, S., Mongkolthanasarak, W., Wannasutta, R., Pongsa, U., &
718 Chindaprasirt, P. (2018). Effect of Oregano Essential Oil Content on Properties of Green
719 Biocomposites Based on Cassava Starch and Sugarcane Bagasse for Bioactive Packaging.
720 *Journal of Polymers and the Environment*, *26*(1), 311–318. [https://doi.org/10.1007/s10924-](https://doi.org/10.1007/s10924-017-0957-x)
721 [017-0957-x](https://doi.org/10.1007/s10924-017-0957-x)

722 Kim, J. D., Kim, J. H., Lee, D. H., Yeom, D. J., & Lee, J. M. (2021). Synthesis and investigation of
723 cryogenic mechanical properties of chopped-glass-fiber-reinforced polyisocyanurate foam.
724 *Materials*, *14*(2), 1–18. <https://doi.org/10.3390/ma14020446>

725 Lai, C. S., Guetzlaff, J., & Hosney, R. C. (1989). Role of sodium bicarbonate and trapped air in
726 extrusion. *Cereal Chemistry*, *66*(2), 69–73.

727 Liu, F., Zhang, Y., Xiao, X., Cao, Y., Jiao, W., Bai, H., Yu, L., & Duan, Q. (2023). Effects of polyvinyl
728 alcohol content and hydrolysis degree on the structure and properties of extruded starch-
729 based foams. *Chemical Engineering Journal*, 472, 144959.

730 Lopez-Gil, A., Silva-Bellucci, F., Velasco, D., Ardanuy, M., & Rodriguez-Perez, M. A. (2015).
731 Cellular structure and mechanical properties of starch-based foamed blocks reinforced
732 with natural fibers and produced by microwave heating. *Industrial Crops and Products*, 66,
733 194–205. <https://doi.org/10.1016/j.indcrop.2014.12.025>

734 Lopresti, F., Botta, L., Scaffaro, R., Bilello, V., Settanni, L., & Gaglio, R. (2019). Antibacterial
735 biopolymeric foams: Structure–property relationship and carvacrol release kinetics.
736 *European Polymer Journal*, 121. <https://doi.org/10.1016/j.eurpolymj.2019.109298>

737 Mali, S., Debiagi, F., Grossmann, M. V. E., & Yamashita, F. (2010). Starch, sugarcane bagasse
738 fibre, and polyvinyl alcohol effects on extruded foam properties: A mixture design
739 approach. *Industrial Crops and Products*, 32(3), 353–359.
740 <https://doi.org/10.1016/j.indcrop.2010.05.014>

741 Merino, D., & Athanassiou, A. (2023). Alkaline hydrolysis of biomass as an alternative green
742 method for bioplastics preparation: In situ cellulose nanofibrillation. *Chemical Engineering*
743 *Journal*, 454, 140171.

744 Mestres, C., Matencio, F., Pons, B., Yajid, M., & Fliedel, G. (1996). A rapid method for the
745 determination of amylose content by using differential-scanning calorimetry. *Starch-Stärke*,
746 48(1), 2–6.

747 Miranda-Valdez, I. Y., Coffeng, S., Zhou, Y., Viitanen, L., Hu, X., Jannuzzi, L., Puisto, A., Kostinen,
748 M. A., Mäkinen, T., Koivisto, J., & Alava, M. J. (2023). Foam-formed biocomposites based on
749 cellulose products and lignin. *Cellulose*, 30(4), 2253–2266.
750 <https://doi.org/10.1007/s10570-022-05041-3>

751 Mu, B., & Yang, Y. (2022). Complete separation of colorants from polymeric materials for cost-
752 effective recycling of waste textiles. *Chemical Engineering Journal*, 427.
753 <https://doi.org/10.1016/j.cej.2021.131570>

754 Naik, T. P., Singh, I., & Sharma, A. K. (2022). Processing of polymer matrix composites using
755 microwave energy: A review. In *Composites Part A: Applied Science and Manufacturing*
756 (Vol. 156). Elsevier Ltd. <https://doi.org/10.1016/j.compositesa.2022.106870>

757 Négrier, M., El Ahmar, E., Sescousse, R., Sauceau, M., & Budtova, T. (2023). Upcycling of textile
758 waste into high added value cellulose porous materials, aerogels and cryogels. *RSC*
759 *Sustainability*, 1(2), 335–345. <https://doi.org/10.1039/d2su00084a>

760 Ou, R., Xie, Y., Wolcott, M. P., Yuan, F., & Wang, Q. (2014). Effect of wood cell wall composition
761 on the rheological properties of wood particle/high density polyethylene composites.
762 *Composites Science and Technology*, 93, 68–75.
763 <https://doi.org/10.1016/j.compscitech.2014.01.001>

764 Pang, M. M., Pun, M. Y., Chow, W. S., & Ishak, Z. A. M. (2014). Carbon footprint calculation for
765 thermoformed starch-filled polypropylene biobased materials. *Journal of Cleaner*
766 *Production*, 64, 602–608. <https://doi.org/10.1016/j.jclepro.2013.07.026>

767 Peltola, H., Pääkkönen, E., Jetsu, P., & Heinemann, S. (2014). Wood based PLA and PP
768 composites: Effect of fibre type and matrix polymer on fibre morphology, dispersion and
769 composite properties. *Composites Part A: Applied Science and Manufacturing*, 61, 13–22.
770 <https://doi.org/10.1016/j.compositesa.2014.02.002>

771 Peng, S., Li, F., Man, J., Li, J., Zhang, C., Ji, M., Li, J., & Wang, S. (2022). Enhancing the properties
772 of starch-fiber foaming material by adjusting fiber length: The synergistic effect of macro-
773 micro stress conduction. *Materials Today Communications*, 33, 104408.

774 Peng, X. W., Ren, J. L., Zhong, L. X., Cao, X. F., & Sun, R. C. (2011). Microwave-induced synthesis
775 of carboxymethyl hemicelluloses and their rheological properties. *Journal of Agricultural
776 and Food Chemistry*, 59(2), 570–576. <https://doi.org/10.1021/jf1036239>

777 Pinto, J., Dumon, M., Pedros, M., Reglero, J., & Rodriguez-Perez, M. A. (2014). Nanocellular CO2
778 foaming of PMMA assisted by block copolymer nanostructuring. *Chemical Engineering
779 Journal*, 243, 428–435. <https://doi.org/10.1016/j.cej.2014.01.021>

780 Poilâne, C., Cherif, Z. E., Richard, F., Vivet, A., Ben Doudou, B., & Chen, J. (2014). Polymer
781 reinforced by flax fibres as a viscoelastoplastic material. *Composite Structures*, 112(1), 100–
782 112. <https://doi.org/10.1016/j.compstruct.2014.01.043>

783 Prabhakar, M. N., Rehman Shah, A. ur, & Song, J. Il. (2017). Improved flame-retardant and
784 tensile properties of thermoplastic starch/flax fabric green composites. *Carbohydrate
785 Polymers*, 168, 201–211. <https://doi.org/10.1016/j.carbpol.2017.03.036>

786 Prachayawarakorn, J., Ruttanabus, P., & Boonsom, P. (2011). Effect of Cotton Fiber Contents and
787 Lengths on Properties of Thermoplastic Starch Composites Prepared from Rice and Waxy
788 Rice Starches. *Journal of Polymers and the Environment*, 19(1), 274–282.
789 <https://doi.org/10.1007/s10924-010-0273-1>

790 Quilez-Molina, A. I., Chandra Paul, U., Merino, D., & Athanassiou, A. (2022). Composites of
791 Thermoplastic Starch and Lignin-Rich Agricultural Waste for the Packaging of Fatty Foods.
792 *ACS Sustainable Chemistry & Engineering*.
793 <https://doi.org/10.1021/acssuschemeng.2c04326>

794 Quilez-Molina, A. I., Heredia-Guerrero, J. A., Armirotti, A., Paul, U. C., Athanassiou, A., & Bayer, I.
795 S. (2020). Comparison of physicochemical, mechanical and antioxidant properties of
796 polyvinyl alcohol films containing green tealeaves waste extracts and discarded balsamic
797 vinegar. *Food Packaging and Shelf Life*, 23. <https://doi.org/10.1016/j.fpsl.2019.100445>

798 Quilez-Molina, A. I., Mazzon, G., Athanassiou, A., & Perotto, G. (2022). A Novel Approach to
799 Fabricate Edible and Heat Sealable Bio-based Films from Vegetable Biomass Rich in Pectin.
800 *Materials Today Communications*, 103871.
801 <https://doi.org/10.1016/j.mtcomm.2022.103871>

802 Quilez-Molina, A. I., Oliveira-Salmazo, L., Amezáa-Arranz, C., López-Gil, A., & Rodríguez-Pérez,
803 M. Á. (2023). Evaluation of the acid hydrolysis as pre-treatment to enhance the integration
804 and functionality of starch composites filled with rich-in-pectin agri-food waste orange
805 peel. *Industrial Crops and Products*, 205, 117407.

806 Robin, F., Engmann, J., Pineau, N., Chanvrier, H., Bovet, N., & Valle, G. Della. (2010). Extrusion,
807 structure and mechanical properties of complex starchy foams. *Journal of Food
808 Engineering*, 98(1), 19–27. <https://doi.org/10.1016/j.jfoodeng.2009.11.016>

809 Rodríguez-Fabià, S., Zarna, C., & Chinga-Carrasco, G. (2023). A comparative study of kraft pulp
810 fibres and the corresponding fibrillated materials as reinforcement of LDPE- and HDPE-
811 biocomposites. *Composites Part A: Applied Science and Manufacturing*, 173.
812 <https://doi.org/10.1016/j.compositesa.2023.107678>

813 Saed Hussein, M., Leng, T. P., Rahmat, A. R., Zainuddin, F., Cheow Keat, Y., Suppiah, K., & Salem
814 Alsagayar, Z. (2019). The effect of sodium bicarbonate as blowing agent on the mechanical

815 properties of epoxy. In *Materials Today: Proceedings* (Vol. 16).
816 www.sciencedirect.comwww.materialstoday.com/proceedings2214-7853

817 Scarlat, N., Prussi, M., & Padella, M. (2022). Quantification of the carbon intensity of electricity
818 produced and used in Europe. *Applied Energy*, 305.
819 <https://doi.org/10.1016/j.apenergy.2021.117901>

820 Soykeabkaew, N., Supaphol, P., & Rujiravanit, R. (2004). Preparation and characterization of jute-
821 and flax-reinforced starch-based composite foams. *Carbohydrate Polymers*, 58(1), 53–63.
822 <https://doi.org/10.1016/j.carbpol.2004.06.037>

823 Soykeabkaew, N., Thanomsilp, C., & Suwanton, O. (2015). A review: Starch-based composite
824 foams. In *Composites Part A: Applied Science and Manufacturing* (Vol. 78, pp. 246–263).
825 Elsevier Ltd. <https://doi.org/10.1016/j.compositesa.2015.08.014>

826 Tacha, S., Somord, K., Rattanawongkun, P., Intatha, U., Tawichai, N., & Soykeabkaew, N. (2023).
827 Bio-nanocomposite foams of starch reinforced with bacterial nanocellulose fibers.
828 *Materials Today: Proceedings*, 75, 119–123. <https://doi.org/10.1016/j.matpr.2022.12.049>

829 Tran, T., Da, G., Moreno-Santander, M. A., Vélez-Hernández, G. A., Giraldo-Toro, A.,
830 Piyachomkwan, K., Sriroth, K., & Dufour, D. (2015). A comparison of energy use, water use
831 and carbon footprint of cassava starch production in Thailand, Vietnam and Colombia.
832 *Resources, Conservation and Recycling*, 100, 31–40.
833 <https://doi.org/10.1016/j.resconrec.2015.04.007>

834 van Rijswijk, K., & Bersee, H. E. N. (2007). Reactive processing of textile fiber-reinforced
835 thermoplastic composites - An overview. In *Composites Part A: Applied Science and*
836 *Manufacturing* (Vol. 38, Issue 3, pp. 666–681).
837 <https://doi.org/10.1016/j.compositesa.2006.05.007>

838 Völtz, L. R., Berglund, L., & Oksman, K. (2023). Resource-efficient manufacturing process of
839 composite materials: Fibrillation of recycled textiles and compounding with thermoplastic
840 polymer. *Composites Part A: Applied Science and Manufacturing*, 175, 107773.
841 <https://doi.org/10.1016/j.compositesa.2023.107773>

842 Wang, Y., Bai, Y., Ji, H., Dong, J., Li, X., Liu, J., & Jin, Z. (2022). Insights into rice starch degradation
843 by maltogenic α -amylase: Effect of starch structure on its rheological properties. *Food*
844 *Hydrocolloids*, 124. <https://doi.org/10.1016/j.foodhyd.2021.107289>

845 Wani, A. A., Singh, P., Shah, M. A., Schweiggert-Weisz, U., Gul, K., & Wani, I. A. (2012). Rice
846 Starch Diversity: Effects on Structural, Morphological, Thermal, and Physicochemical
847 Properties-A Review. In *Comprehensive Reviews in Food Science and Food Safety* (Vol. 11,
848 Issue 5, pp. 417–436). <https://doi.org/10.1111/j.1541-4337.2012.00193.x>

849 Wei, Q. Y., Fang, Y. D., Sun, Z. B., Zeng, Y., Zhang, J., Lei, J., Xu, L., Lin, H., Zhong, G. J., & Li, Z. M.
850 (2023). Fabrication of PLA/CB composites with excellent electrical conductivity and
851 stiffness-ductility balance based on coupling extensional stress with thermal field.
852 *Composites Part A: Applied Science and Manufacturing*, 169.
853 <https://doi.org/10.1016/j.compositesa.2023.107516>

854 Xie, Y., Yan, M., Yuan, S., Sun, S., & Huo, Q. (2013). Effect of microwave treatment on the
855 physicochemical properties of potato starch granules. *Chemistry Central Journal*, 7(1), 1–7.

856 Yildirim, N., Shaler, S. M., Gardner, D. J., Rice, R., & Bousfield, D. W. (2014). Cellulose nanofibril
857 (CNF) reinforced starch insulating foams. *Cellulose*, 21(6), 4337–4347.
858 <https://doi.org/10.1007/s10570-014-0450-9>

859 Yu, I. K. M., Chen, H., Abeln, F., Auta, H., Fan, J., Budarin, V. L., Clark, J. H., Parsons, S., Chuck, C.
860 J., Zhang, S., Luo, G., & Tsang, D. C. W. (2021). Chemicals from lignocellulosic biomass: A
861 critical comparison between biochemical, microwave and thermochemical conversion
862 methods. *Critical Reviews in Environmental Science and Technology*, 51(14), 1479–1532.
863 <https://doi.org/10.1080/10643389.2020.1753632>

864 Zhang, J., Liu, B., Zhou, Y., Essawy, H., Zhao, C., Wu, Z., Zhou, X., Hou, D., & Du, G. (2022).
865 Gelatinized starch-furanic hybrid as a biodegradable thermosetting resin for fabrication of
866 foams for building materials. *Carbohydrate Polymers*, 298.
867 <https://doi.org/10.1016/j.carbpol.2022.120157>

868 Zhang, L., Zhao, J., Zhang, Y., Li, F., Jiao, X., & Li, Q. (2021). The effects of cellulose nanocrystal
869 and cellulose nanofiber on the properties of pumpkin starch-based composite films.
870 *International Journal of Biological Macromolecules*, 192, 444–451.
871 <https://doi.org/10.1016/j.ijbiomac.2021.09.187>

872 Zhang, Q., Wang, Z., Zhang, C., Aluko, R. E., Yuan, J., Ju, X., & He, R. (2020). Structural and
873 functional characterization of rice starch-based superabsorbent polymer materials.
874 *International Journal of Biological Macromolecules*, 153, 1291–1298.
875 <https://doi.org/10.1016/j.ijbiomac.2019.10.264>

876 Zhang, Z. X., Zhang, J., Lu, B. X., Xin, Z. X., Kang, C. K., & Kim, J. K. (2012). Effect of flame
877 retardants on mechanical properties, flammability and foamability of PP/wood-fiber
878 composites. *Composites Part B: Engineering*, 43(2), 150–158.
879 <https://doi.org/10.1016/j.compositesb.2011.06.020>

880 Zhou, Y. G., & Zhang, Y. L. (2023). Hybrid reinforced effect of long carbon fiber and short glass
881 fiber on polycarbonate foams. *Polymer Composites*. <https://doi.org/10.1002/pc.27578>

882 Zimmermann, M. V. G., da Silva, M. P., Zattera, A. J., & Campomanes Santana, R. M. (2017).
883 Effect of nanocellulose fibers and acetylated nanocellulose fibers on properties of
884 poly(ethylene-co-vinyl acetate) foams. *Journal of Applied Polymer Science*, 134(17).
885 <https://doi.org/10.1002/app.44760>

886 Zimniewska, M., Rożańska, W., Gryszczynska, A., Romanowska, B., & Kicinska-Jakubowska, A.
887 (2018). Antioxidant potential of hemp and flax fibers depending on their chemical
888 composition. *Molecules*, 23(8). <https://doi.org/10.3390/molecules23081993>

889 Zuo, Y., Gu, J., Tan, H., Qiao, Z., Xie, Y., & Zhang, Y. (2014). The characterization of granule
890 structural changes in acid-thinning starches by new methods and its effect on other
891 properties. *Journal of Adhesion Science and Technology*, 28(5), 479–489.
892 <https://doi.org/10.1080/01694243.2013.843283>

893